Chinese Chemical Letters 34 (2023) 107540

Contents lists available at ScienceDirect

Chinese Chemical Letters

journal homepage: www.elsevier.com/locate/cclet

Hydrated ammonium manganese phosphates by electrochemically induced manganese-defect as cathode material for aqueous zinc ion batteries

Xiangsi Wu[a,b,1], Guangli Liu[b,1], Sinian Yang[b], Yuting Li[b], Hongqiang Wang[a], Qingyu Li[a,*], Xianwen Wu[b,*]

[a] Guangxi Key Laboratory of Low Carbon Energy Materials, School of Chemical and Pharmaceutical Science, Guangxi New Energy Ship Battery Engineering Technology Research Center, Guangxi Normal University, Guilin 541004, China
[b] School of Chemistry and Chemical Engineering, Jishou University, Jishou 416000, China

ARTICLE INFO

Article history:
Received 9 April 2022
Revised 1 May 2022
Accepted 17 May 2022
Available online 20 May 2022

Keywords:
Rechargeable aqueous zinc ion batteries
Athode materials
Manganese-based compounds
Cationic defect
Electrochemical storage mechanism

ABSTRACT

Aqueous zinc ion batteries (AZIBs) with the merits of low cost, low toxicity, high safety, environmental benignity as well as multi-valence properties as the large-scale energy storage devices demonstrate tremendous application prospect. However, the explorations for the most competitive manganese-based cathode materials of AZIBs have been mainly limited to some known manganese oxides. Herein, we report a new type of cathode material $NH_4MnPO_4{\cdot}H_2O$ (abbreviated as AMPH) for rechargeable AZIBs synthesized through a simple hydrothermal method. An *in-situ* electrochemical strategy inducing Mn-defect has been used to unlock the electrochemical activity of AMPH through the initial charge process, which can convert poor electrochemical characteristic of AMPH towards Zn^{2+} and NH_4^+ into great electrochemically active cathode for AZIBs. It still delivers a reversible discharge capacity up to 90.0 mAh/g at 0.5 A/g even after 1000^{th} cycles, which indicates a considerable capacity and an impressive cycle stability. Furthermore, this cathode reveals an (de)insertion mechanism of Zn^{2+} and NH_4^+ without structural collapse during the charge/discharge process. The work not only supplements a new member for the family of manganese-based compound for AZIBs, but also provides a potential direction for developing novel cathode material for AZIBs by introducing defect chemistry.

With the increasing consumption and depletion of conventional fossil energy, the ongoing energy crisis attracted extensive attention from the researchers in the past decades. Nowadays there are clear timetable and roadmap about China's carbon emission peak and carbon neutral plans. Accordingly, renewable green and clean energy have been continually developed, such as solar energy and nuclear energy [1–3]. As is known that the supercapacitors and rechargeable battery systems can reduce the use of finite fossil fuels and convert the chemical energy to the electric energy [4–8]. Therefore, researchers have always been seeking for novel energy storage devices with high energy densities and safety characteristics [9–11]. Among them, rechargeable lithium ion batteries have dominated a major part of the market in the portable electronic devices such as mobile phones on account of their remarkable energy density, very high power density, and excellent life span [12–14]. However, their practical application has been restricted by the high cost, lithium sources shortage and safety risks. Compared with lithium ion batteries with organic electrolyte, rechargeable aqueous lithium/sodium/zinc ion batteries (ALIBs/ANIBs/AZIBs) [15–19] and rechargeable hybrid aqueous batteries (ReHABs) are equipped with low cost, high power density, high safety and superior ecofriendliness [20].

Among the reported aqueous batteries at present, aqueous zinc ion batteries (AZIBs) in a neutral or weak acid system have brought about extensive interests and are thought to be one of the most promising generation energy storage devices [21–26]. It could date back to $Zn/ZnSO_4/MnO_2$ system which firstly proposed by Yamamoto and Shoji in 1986 [27]. More importantly, AZIBs possess much merits such as the multivalent characteristic, low cost, low redox potential (−0.76 V *vs.* SHE), convenient assembly, abundant resources, environmental benignity, long cycle life and inexpensive of Zn metal [28]. Although great efforts have been devoted to the exploration of electrode materials and their related energy storage mechanisms about AZIBs, the tremendous challenges still

* Corresponding authors.
E-mail addresses: 13975808173@126.com (Q. Li), wxwcsu2011@163.com (X. Wu).
[1] These authors contributed equally to this work.

https://doi.org/10.1016/j.cclet.2022.05.054
1001-8417/

remain in exploring high-performance AZIBs [29–35]. To be more specific, one of the major problems is lack of appropriate cathode material. As mentioned above, the associated cathode materials mainly include manganese-based, vanadium-based and other cathode materials [36–41]. Nevertheless, the attractive manganese-based materials demonstrate the tremendous application prospect in AZIBs. Wherein, various manganese oxides with many valence such as Mn_2O_3, (α-, β-, γ-, δ-, ε-, λ-type) MnO_2, MnO, $ZnMn_2O_4$, $ZnMn_2O_4/Mn_2O_3$ have been reported successively [42–46]. However, their intrinsic low electronic conductivity and the inevitable manganese dissolution phenomenon will lead to their terrible rate characteristic, fast capacity fading and poor cycling stability.

Recently, $NH_4MnPO_4{\cdot}H_2O$ as the electrode material was investigated for supercapacitor, and its layered crystal structure with ion channels may be suitable for zinc ion intercalation/deintercalation [47]. Inspired by this idea, in this work we try to prepare a novel cathode material of $NH_4MnPO_4{\cdot}H_2O$ for AZIBs which is fabricated through a simple hydrothermal method. An *in-situ* electrochemical approach inducing manganese-defect will be used to unlock the electrochemical activity of AMPH through the initial charge process for the first time, which can convert terrible electrochemical characteristic of AMPH towards Zn^{2+} and NH_4^+ into high electrochemically active cathode for AZIBs. Finally, we expect that AMPH will demonstrate a considerable capacity and superior cycleability when used as the cathode material for AZIBs. Meanwhile, we will reveal the clear energy storage mechanism by the typical *ex-situ* X-ray diffraction and X-ray photoelectron spectroscopy characterizations.

In order to investigate thermal decomposition process and confirm the content of crystal water in the hydrates, TG analysis of the target product was characterized in air from 30 °C to 800 °C at a heating rate of 10 °C/min. As shown in Fig. 1a, it records two-step weight loss. About 19.8 wt% of weight loss in the steep region from 180 °C to 314.7 °C is mainly assigned to the evaporation of adsorbed water and dehydration of compound. While another significant one about 4.3 wt% occurs in the gradual region up to 527.7 °C, which is mainly assigned to the removal of NH_3 and H_2O and the subsequent dehydration condensation during the thermal decomposition process of AMPH. In fact, AMPH is firstly decomposed to amorphous $MnHPO_4$ phase and then transformed into $Mn_2P_2O_7$ according to the previous report [47]. The reaction equation can be described as follows.

$$NH_4MnPO_4{\cdot}H_2O \rightarrow MnHPO_4{+}NH_3{+}H_2O \quad (1)$$

$$2MnHPO_4 \rightarrow Mn_2P_2O_7{+}H_2O \quad (2)$$

The phase composition and purity of hydrated ammonium manganese phosphates (AMPH) sample was firstly characterized by traditional X-ray diffraction (XRD), as shown in Fig. 1b**.** It is obvious that two prominent peaks with higher intensity at 10.11° and 31.47° can be observed, which are consistent with (010) and (121) planes. Meanwhile, all the other weak or tiny satellite peaks detected at 18.49°, 20.71°, 25.92°, 36.59°, 39.05° correspond well to the (110), (011), (111), (002), (131) and (240) of AMPH with layered crystal structure (PDF# 50-0554), demonstrating the successful synthesis of pure AMPH with better crystallinity [48]. The calculated crystallite size of (010) crystal plane with Scherrer's formula reveals about 158.2 nm for AMPH.

To further characterize the functional groups of AMPH powder, FT-IR measurement was verified carefully. As shown in Fig. 1c, a large band at 3410 cm^{-1} is ascribed to the O–H stretches of water molecules in the hydrates, whereas the band located at 1620 cm^{-1} is due to the bending vibration of the O–H group. A weak band at about 2800 cm^{-1} and the bands in the region of 1400–1500 cm^{-1} correspond to the N-H symmetric stretching vibration and its bending mode of NH_4^+, respectively. There are also strong bands between 930 and 1130 cm^{-1}. A moderately strong absorption band at 953 cm^{-1} is mainly attributed to the bending vibration of PO_4^{3-}, while the sharp one at 1040 cm^{-1} is well consistent with the asymmetrical stretching vibration of PO_4^{3-}. In addition, a characteristic absorption band in the region below 740 cm^{-1} corresponds to Mn–O bond. All of these reveals the typical presence of ammonium manganese phosphates with crystal water, which matches well with that described in previous report [48]. Furthermore, the homogeneous distribution of N, P, Mn and O elements in the cathode material can be shown from the SEM-EDS element mappings in Figs. 1d–h, which is further confirmed the successful synthesis and the uniform growth of AMPH.

Subsequently, the surface element states and the element composition presented in AMPH sample were further analyzed by high-resolution XPS characterization, which were in combination with the XPS peak software. As displayed in Fig. 2a, the survey spectra of AMPH cathode demonstrates the presence of N, Mn, P and O as well as C elements, which is consistent with SEM-EDS test, implying the pure phase of AMPH. Meanwhile, the binding energy peak at 641.4 eV in Fig. 2b associated with Mn $2p_{3/2}$ reveals the Mn(II) oxidation state, which are the characteristics of AMPH [49]. Meanwhile, the fitting results of the deconvoluted peaks in Mn $2p_{3/2}$ spectra can be confirmed the multiple Mn valences in Fig. 2b, which may be the formation of deficient AMPH. The main peak located at 133.2 eV in Fig. 2c is ascribed to P 2p states of

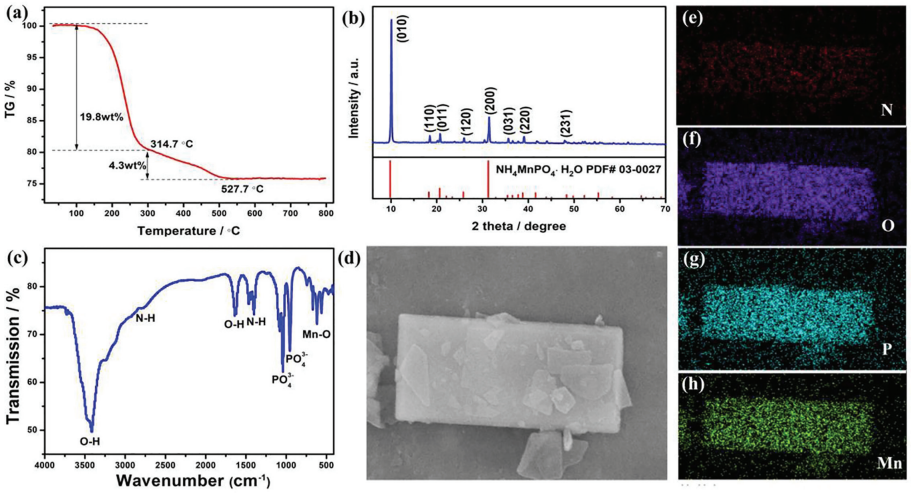

Fig. 1. (a) TG curve of AMPH in air. (b) XRD pattern of AMPH. (c) FTIR spectrums of AMPH and (d–h) the corresponding mapping images of AMPH.

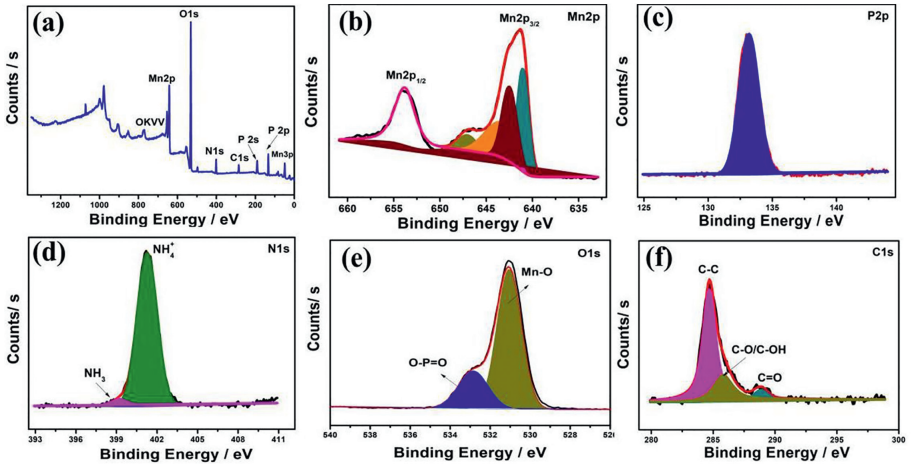

Fig. 2. XPS spectra of AMPH: (a) Survey spectrum, (b) Mn 2p, (c) P 2p, (d) N 1s, (e) O 1s, (f) C 1s.

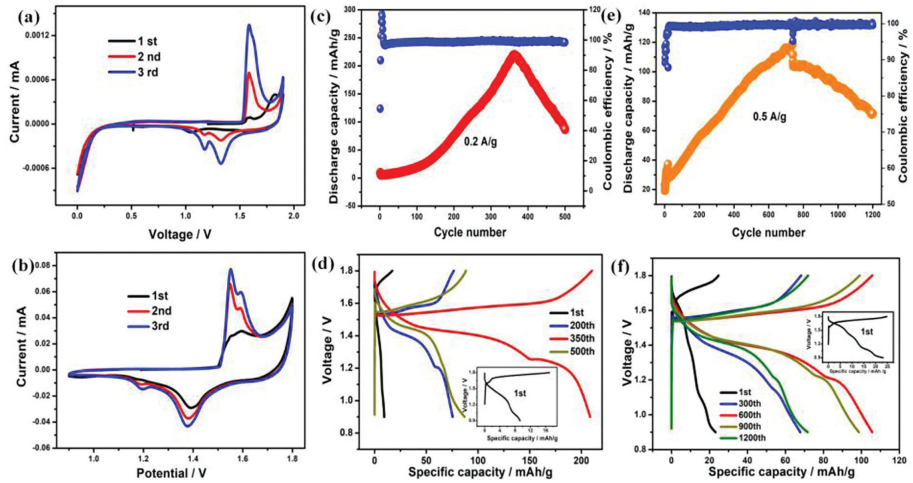

Fig. 3. The cyclic voltammetry of different cut-off voltages (a) 0–1.9 V and (b) 0.9–1.8 V. The cycling performance and charge/discharge curves at different current densities: (c, d) 0.2 A/g and (e, f) 0.5 A/g.

phosphate complexation. Additionally, the presence of NH_3 and NH_4^+ compositions at 399.2 eV and 401.3 eV, respectively, is in good agreement with the characteristics of typical N 1s states in Fig. 2d. As shown in Fig. 2e, the deconvoluted O 1s spectrum can be fitted with two sub-peaks. The first one at 531.1 eV matches well with the state of oxygen bonding with Mn^{2+}, the second one at 532.8 eV is attributed to the typical phosphorus-oxygen bond in the as-prepared materials. In addition, the high-resolution C1s spectrum is often used as the reference for calibration in Fig. 2f [50].

The morphology of the as-synthesized AMPH is shown by SEM and TEM images in Figs. S2a–d (Supporting information). It appears as clusters of flakes with the size of about 300 nm in thickness, 0.5–1 μm in width and 1–2 μm in length, which demonstrates rectangular parallelepiped shape distinctly. The HRTEM images of AMPH in Figs. S2e–h (Supporting information) reveal the interplanar spacing of about 0.2137, 0.2826, 0.2465 and 0.255 nm, corresponding to the (112), (200), (002) and (031) planes of AMPH.

Moreover, a novel AZIBs were constructed for the first time based on Zn//AMPH, and a series of electrochemical performances have been evaluated though cyclic voltammetry (CV) and galvanostatic charge/discharge tests using 2 mol/L $ZnSO_4$ as the electrolyte. Firstly, in order to confirm the cut-off voltage of charge/discharge, the CV curve was measured at 0.1 mV/s in the potential range of 0.0–1.9 V *vs.* Zn^{2+}/Zn in Fig. 3a. Obviously, except the typical redox peaks corresponding to the electrochemical active substance of manganese, there exist oxygen and hydrogen evolution at high and low potentials, respectively. As shown in Fig. 3b, two main pairs of redox peaks observed at 1.07/0.98 V and 0.60/0.45 V, respectively, reflects a possible multistep (de)intercalation of ions from/into AMPH framework. Importantly, the CV profile is the same as that frequently reported in other manganese-based cathodes [24]. Notably, the corresponding peak current rising gradually and the stable position of redox peaks with the lap increasing demonstrate the high reversibility of the electrode, implying an excellent cycling stability and the increasing-gradually charge/discharge capacity of AZIBs, which is related to the continuous activation of the AMPH.

To further reveal the typical electrochemical behavior, the galvanostatic charge/discharge data were collected at different current densities, as depicted in Figs. 3c–f. Surprisingly, the specific discharge capacity upon cycling increases quickly in the beginning, which should be ascribed to the sustainable activation process, and then shows a decreasing trend. It very looks like a parabolic curve in mathematics. Accurately, the initial reversible discharge capacity of 9.3 mAh/g with the coulombic efficiency of only 54.5% is delivered by AMPH at 0.2 A/g. Remarkably, it even achieves as much as 219.6 mAh/g after 363th cycles, corresponding to nearly 100% of the coulombic efficiency. AMPH electrode still retains 86.9 mAh/g of the reversible capacity even after 500th cycles, which is much

higher than that initial one. As observed from the charge/discharge curves at different cycles in Fig. 3d, the charge plateau decreases and the discharge plateau increases gradually, suggesting the low overpotential. Notably, two obvious discharge plateaus during the capacity rising stage transforms into only one during the significant capacity decay process. Importantly, as the current density increases to 0.5 A/g, the shape of the cycling curve keeps the same as that at 0.2 A/g, and it still delivers a reversible capacity up to 90.0 mAh/g even after 1000th cycles, which is much higher than that at 0.2 A/g.

Finally, the electrochemical energy storage mechanism of Zn//AMPH battery was further assessed in Fig. S4 (Supporting information), *ex-situ* XRD measurements are carried out in different state of charge for batteries after cycled 100 times by exploring and observing the structural changes and phase evolution of AMPH. Interestingly, all of the main diffraction peaks of *ex-situ* XRD can be well in agreement with the standard patterns of AMPH (PDF#03-0027), demonstrating a stable structure of AMPH without phase transformation and structural collapse during energy storage process in Fig. S4a. However, it is observed that the new diffraction peaks with 2θ at 20.246° and so on are accordance with $[Zn(OH)_2]_3(ZnSO_4)\cdot 5H_2O$ (PDF#78-0246, ZHS). Meanwhile, the other diffraction peaks with 2θ at 20.246°, 22.112° belongs to $ZnSO_4\cdot 6H_2O$(PDF#75-0949).

In fact, during the early charge stage, a part of NH_4^+ are deintercalated from AMPH framework and dissolved into the electrolyte, and Mn(II) undergoes an electrochemical oxidation reaction, accompanied by releasing electrons. Wherein a small amount of Mn defects because of the dissolution of Mn^{2+} were produced during the charge process that converts the AMPH with terrible electrochemical activities towards Zn^{2+} into excellent active cathode for AZIBs, which can be confirmed by inductively coupled plasma optical emission spectrometer (abbreviated as ICP-OES) test in the electrolyte. The similar electrochemical characteristics can be observed in the bivalent manganese-based compound [44]. Mn defects and NH_4^+ deintercalation are also indicative of the new phase formation of $[Zn_3(PO_4)]_2\cdot 4H_2O$ due to the subsequent intercalation of zinc ions. More importantly, the Mn dissolution tends to establish balance, which will suppress continuous Mn^{2+} dissolution. In the case of discharge and following cycles, a few NH_4^+ and Mn^{2+} exist in the electrolyte, abundant Zn^{2+} and a few NH_4^+ can intercalate/deintercalate into/from the cathode material of AMPH matrix. In addition, a series of other diffraction peaks at approximate 9.638°, 19.344° and 26.213° are mainly attributed to $[Zn_3(PO_4)]_2\cdot 4H_2O$ (PDF#70-0900). It is noted that the characteristic diffraction peak of ZHS during the discharge process in Fig. S4b shifts to low diffraction angle, indicating the shrinkage of cell, which may be attributed to continuous intercalation of Zn^{2+} and NH_4^+ into AMPH. To verify the energy storage mechanism, XPS test was further used to reveal the change of element contents in the cathode during charge/discharge process in Fig. S5 (Supporting information). Obviously, the peak intensity of N 1s and Zn 2p increase a lot from charging to discharging process. However, there is no much change for the content of Mn 2p peak, attributed to the simultaneous (de)intercaltion of Zn^{2+} and NH_4^+.

Based on the above preliminary analysis and study, significant insight into the energy storage mechanism of AMPH cathode in AZIBs is illustrated in Fig. 4. AMPH cathode with layered crystal structure demonstrated an insertion/extraction mechanism without structural collapse during co-inertion of Zn^{2+} and NH_4^+. An electrochemical charge process with *in-situ* induced Mn-defect converts the AMPH with poor electrochemical activities towards Zn^{2+} and NH_4^+ into excellent active cathode for AZIBs. The presence of Mn defects provides enough diffusion channels and abundant active sites for Zn^{2+} and NH_4^+. The dissolved Mn^{2+} will further inhibit significantly continuous Mn^{2+} dissolution in turn.

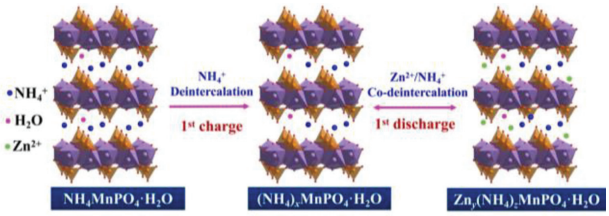

Fig. 4. Schematic of Zn^{2+} and NH_4^+ co-(de)intercalation into/from $NH_4MnPO_4\cdot H_2O$ cathode during cycling.

In summary, we have synthesized $NH_4MnPO_4\cdot H_2O$ successfully through a simple hydrothermal method. More importantly, we firstly report a potential cathode material of AMPH with ion channels for AZIBs. The active AMPH by an electrochemical approach inducing Mn-defect indicates a considerable capacity although the cycling performance should be improved. The charge storage kinetics analysis reveals that the high reversibility is mainly associated with the surface-controlled capacitive behavior. Furthermore, the AMPH cathode exhibits an (de)insertion mechanism for Zn^{2+} and NH_4^+ without structural collapse during the charge/discharge process. We really hope the preliminary work can bring some new ideas and pave the pathway for designing cathode materials and further investigating green, safe, low-cost and high-performance AZIBs for future large-scale application.

Declaration of competing interest

The authors declare that they have no known competing financial interests or personal relationships that could have appeared to influence the work reported in this paper.

Acknowledgments

This research was financially supported by the National Natural Science Foundation of China (Nos. 52064013, 52064014) and Research Innovation Project of Undergraduate for Hunan Province (No. S202110531061), which were greatly appreciated.

Supplementary materials

Supplementary material associated with this article can be found, in the online version, at doi:10.1016/j.cclet.2022.05.054.

References

[1] P. Chen, F. Liu, H.Z. Ding, et al., Appl. Catal. B: Environ. 252 (2019) 33–40.
[2] S.P. Tang, Z.H. Fu, Y. Li, Y.J. Li, Appl. Catal. A: Gen. 590 (2020) 117342.
[3] F.Z. Li, J.S. Li, Q.J. Feng, et al., J. Energy Chem. 27 (2018) 419–425.
[4] T.F. Yi, L.Y. Qiu, J. Mei, et al., Sci. Bull. 65 (2020) 546–556.
[5] Z.D. Huang, T.R. Wang, H. Song, et al., Angew. Chem. Int. Ed. 133 (2021) 1024–1034.
[6] P. Kong, L. Zhu, F.R. Li, G.B. Xu, ChemElectroChem 22 (2019) 5642–5650.
[7] J. Wang, G.Y. Liu, K.L. Fan, et al., J. Colloid Interface Sci. 517 (2018) 134–143.
[8] T.F. Shi, L.N. Shi, X. Han, et al., Energy Environ. Mater. 4 (2021) 586–595.
[9] M. Zhong, J.D. Guan, Q.J. Feng, et al., Carbon 128 (2018) 86–96.
[10] C. Chen, Q.W. Liang, Z.X. Chen, et al., Angew. Chem. Int. Ed. 60 (2021) 26718–26724.
[11] H.W. Fu, Y.P. Wang, G.Z. Fan, et al., Chem. Sci. 13 (2022) 726–736.
[12] D.D. Liu, X.H. Xiong, Q.W. Liang, X.W. Wu, H.K. Fu, Chem. Commun. 57 (2021) 9232–9235.
[13] J.L. Wang, Y. Nie, C. Miao, et al., J. Colloid Interface Sci. 601 (2021) 853–862.
[14] Z. Jiang, Y.H. Li, C. Han, et al., J. Electrochem. Soc. 167 (2020) 020550.
[15] L. Suo, O. Borodin, T. Gao, et al., Science 350 (2015) 938–943.
[16] C. Yang, J. Chen, X. Ji, et al., Nature 569 (2019) 245–250.
[17] D. Bin, F. Wang, A.G. Tamirat, et al., Adv. Energy Mater. 8 (2018) 1703008.
[18] X.W. Wu, F.N. Long, J.B. Jiang, et al., Prog. Chem. 33 (2021) 1983–2001.
[19] Q. Zhang, J.Y. Luan, Y.G. Tang, et al., Angew. Chem Int. Ed. 59 (2020) 13180–13191.
[20] H.B. Zhao, C.J. Hu, H.W. Cheng, et al., Sci. Rep. 6 (2016) 25809.
[21] T.T. Wang, C.P. Li, X.S. Xie, et al., ACS Nano 14 (2020) 16321–16347.

[22] X. Xie, S.Q. Liang, J. Gao, et al., Energy Environ. Sci. 13 (2020) 503–510.
[23] C.P. Li, X.S. Xie, S.Q. Liang, J. Zhou, Energ. Environ. Mater. 3 (2020) 146–159.
[24] S.H. Zhou, X.W. Wu, Y.H. Xiang, et al., Prog. Chem. 33 (2021) 649–669.
[25] F. Wan, L. Zhang, X. Dai, et al., Nat. Commun. 9 (2018) 1656.
[26] B. Li, J. Xue, C. Han, et al., J. Colloid Interface Sci. 599 (2021) 467–475.
[27] T. Yamamoto, T. Shoji, Inorg. Chim. Acta 117 (1986) L27–L28.
[28] B. Tang, L. Shan, S.Q. Liang, J. Zhou, Energy Environ. Sci. 12 (2019) 3288–3304.
[29] D. Kundu, B. Adams, V. Duffort, S. Vajargah, L. Naza, Nat. Energy 1 (2016) 16119.
[30] N. Zhang, X. Chen, M. Yu, et al., Chem. Soc. Rev. 49 (2020) 4203–4219.
[31] F.N. Long, Y.H. Xiang, S.N. Yang, et al., J. Colloid Interface Sci. 616 (2022) 101–109.
[32] W. Sun, F. Wang, S. Hou, et al., J. Am. Chem.Soc. 139 (2017) 9775–9778.
[33] Y.H. Dai, X.B. Liao, R.H. Yu, et al., Adv. Mater. 33 (2021) 2100359.
[34] T. Xue, H.J. Fan, J. Energy Chem. 54 (2021) 194–201.
[35] C.X. Xu, J.J. Jiang, Rare Met. 40 (2021) 749–751.
[36] T. Xiong, Y.X. Zhang, W.S.V. Li, J.M. Xue, Adv. Energy Mater. 10 (2020) 2001769.
[37] N. Niu, B. Li, Z.X. He, et al., J. Energy Chem. 59 (2021) 134–159.
[38] J.H. Huang, Z.W. Guo, Y.Y. Ma, et al., Small Methods 3 (2018) 1800272.
[39] B. Yong, D.T. Ma, Y.Y. Wang, et al., Adv. Energy Mater. 10 (2020) 2002354.
[40] H.F. Li, L.T. Ma, C.P. Han, et al., Nano Energy 62 (2019) 550–587.
[41] W.Z. Kou, L. Yu, Q. Wang, et al., J. Power Sources 520 (2022) 230872.
[42] N. Zhang, F. Cheng, Y. Liu, et al., J. Am. Chem. Soc. 138 (2016) 12894–12901.
[43] F. Tang, J.Y. Gao, Q.Y. Ruan, et al., Electrochim. Acta 353 (2020) 136570.
[44] H. Pan, Y. Shao, P. Yan, et al., Nat. Energy 1 (2016) 16039.
[45] C. Xu, B. Li, H. Du, F.Y. Kang, Angew. Chem. Int. Ed. 51 (2012) 933–935.
[46] S.N. Yang, M.S. Zhang, X.W. Wu, et al., J. Electroanal. Chem. 832 (2019) 69–74.
[47] T.A. Raja, P. Vickraman, A.S. Justin, B.J. Reddy, J. Mater. Sci. 55 (2020) 14447–14463.
[48] T. Kozawa, K. Fukuyama, A. Kondo, M. Naito, ACS Omega 4 (2019) 5690–5695.
[49] K. Raju, H. Han, D.B. Velusamy, et al., ACS Energy Lett. 5 (2020) 23–30.
[50] X.W. Wu, Y.H. Xiang, Q.J. Peng, et al., J. Mater. Chem. A 5 (2017) 17990–17997.